Article

Neuron

Parvalbumin Interneurons of Hippocampus Tune Population Activity at Theta Frequency

Highlights

- PV interneuron optogenetic activation drives intrinsic HP theta optimally at 8 Hz
- PV interneuron optogenetic silencing disrupts intrinsic theta oscillations
- SOM interneurons are weakly involved in theta generation at the local network level
- SOM interneurons modulate the entrainment of intrinsic theta rhythm by EC inputs

Authors

Bénédicte Amilhon, Carey Y.L. Huh, ..., Antoine Adamantidis, Sylvain Williams

Correspondence

benedicte.amilhon@douglas.mcgill.ca (B.A.),
sylvain.williams@mcgill.ca (S.W.)

In Brief

Amilhon et al. show that parvalbumin-expressing interneurons play a crucial role in intrinsic theta rhythm generation in the hippocampus. Somatostatin-expressing interneurons participate only moderately in theta generation but interact with entorhinal cortex inputs to modulate hippocampal theta rhythm.

Amilhon et al., 2015, Neuron *86*, 1277–1289
June 3, 2015
http://dx.doi.org/10.1016/j.neuron.2015.05.027

CellPress

Neuron
Article

Parvalbumin Interneurons of Hippocampus Tune Population Activity at Theta Frequency

Bénédicte Amilhon,[1,*] Carey Y.L. Huh,[1] Frédéric Manseau,[1] Guillaume Ducharme,[1] Heather Nichol,[1] Antoine Adamantidis,[1,2] and Sylvain Williams[1,*]
[1]Department of Psychiatry, Douglas Mental Health University Institute, McGill University, 6875 Lasalle Boulevard, Montréal, QC H4H 1R3, Canada
[2]Department of Neurology, Inselspital University Hospital, University of Bern, Freiburgstrasse 18, 3010 Bern, Switzerland
*Correspondence: benedicte.amilhon@douglas.mcgill.ca (B.A.), sylvain.williams@mcgill.ca (S.W.)
http://dx.doi.org/10.1016/j.neuron.2015.05.027

SUMMARY

Hippocampal theta rhythm arises from a combination of recently described intrinsic theta oscillators and inputs from multiple brain areas. Interneurons expressing the markers parvalbumin (PV) and somatostatin (SOM) are leading candidates to participate in intrinsic rhythm generation and principal cell (PC) coordination in distal CA1 and subiculum. We tested their involvement by optogenetically activating and silencing PV or SOM interneurons in an intact hippocampus preparation that preserves intrinsic connections and oscillates spontaneously at theta frequencies. Despite evidence suggesting that SOM interneurons are crucial for theta, optogenetic manipulation of these interneurons modestly influenced theta rhythm. However, SOM interneurons were able to strongly modulate temporoammonic inputs. In contrast, activation of PV interneurons powerfully controlled PC network and rhythm generation optimally at 8 Hz, while continuously silencing them disrupted theta. Our results thus demonstrate a pivotal role of PV but not SOM interneurons for PC synchronization and the emergence of intrinsic hippocampal theta.

INTRODUCTION

Theta rhythm provides a temporal metric to single neurons (O'Keefe, 1993; Colgin, 2013) and allows the binding of cell assemblies within and between structures (Seidenbecher et al., 2003; Adhikari et al., 2010). Theta has been extensively studied in the hippocampus, where a combination of cellular properties, local network interactions, and inputs from other brain regions acts together to generate in vivo oscillations. At the single cell level, theta-resonance properties of pyramidal cells (Pike et al., 2000; Stark et al., 2013) and some subtypes of interneurons (Maccaferri and McBain, 1996; Pike et al., 2000) are believed to contribute to the emergence of oscillatory activity. Local network interactions due to perisomatic inhibition in CA1 stratum pyramidale (Soltesz and Deschênes, 1993; Ylinen et al., 1995) and excitatory inputs from the CA3 (Kocsis et al., 1999; Buzsáki, 2002) contribute to the intrinsic hippocampal field potentials. Single cell properties and local network interactions thus constitute a first level of theta rhythm generation, intrinsic to the hippocampal neuronal network. Accordingly, recent work from our laboratory using the isolated in vitro hippocampus has shown that the hippocampus contains two series of intrinsic oscillators, located longitudinally in the distal CA1/subiculum (dCA1/SUB) and CA3 regions (Goutagny et al., 2009; Jackson et al., 2011; Gu et al., 2013; Jackson et al., 2014). A prominent external excitatory input from the entorhinal cortex (EC) also participates in theta oscillations (Kamondi et al., 1998). Therefore, both in vitro and in vivo studies support the view that theta rhythm is generated by interacting intrinsic and external oscillators (Colgin, 2013).

GABAergic interneurons are centrally positioned to integrate internal and external inputs and are therefore considered to be essential for theta generation. However, which interneuron subtypes are instrumental in driving pyramidal cell activity to generate theta oscillations remains unclear. Two interneuron subtypes are considered to be critical in the generation of theta: interneurons expressing the calcium-binding protein parvalbumin (PV) and those expressing the neuropeptide somatostatin (SOM). PV-positive interneurons target the somata and axon initial segments of principal cells (PCs) and thus likely exert powerful control over the output of large populations of PCs (Cobb et al., 1995). Their activity in vivo is tightly phase locked to hippocampal theta and gamma oscillations (Lapray et al., 2012; Varga et al., 2012). It is now well established that PV interneurons have a causal role in cortical gamma oscillation generation in vivo (Cardin et al., 2009; Sohal et al., 2009). Although several studies suggested that PV interneurons are important in the generation of theta oscillations in the hippocampus (Cobb et al., 1995; Ylinen et al., 1995), this has not been shown experimentally (Wulff et al., 2009; Royer et al., 2012). A recent study has shown that optogenetic stimulation of PV interneurons in vivo induces theta-resonance spiking in PYR cells (Stark et al., 2013) further suggesting that PV cells may play a role in theta oscillations. In comparison, interneurons expressing SOM constitute a more complex cell population composed in part by distal dendrite targeting oriens-lacunosum molecular (O-LM) cells (Klausberger and Somogyi, 2008). A role for O-LM interneurons in theta generation has been predicted on the basis of their slow membrane conductance resonating at theta frequency, their intrinsic capacity to spike at theta frequency (Maccaferri and McBain, 1996; Pike et al., 2000) and their firing phase locked to theta oscillations in vivo (Varga et al., 2012). Studies

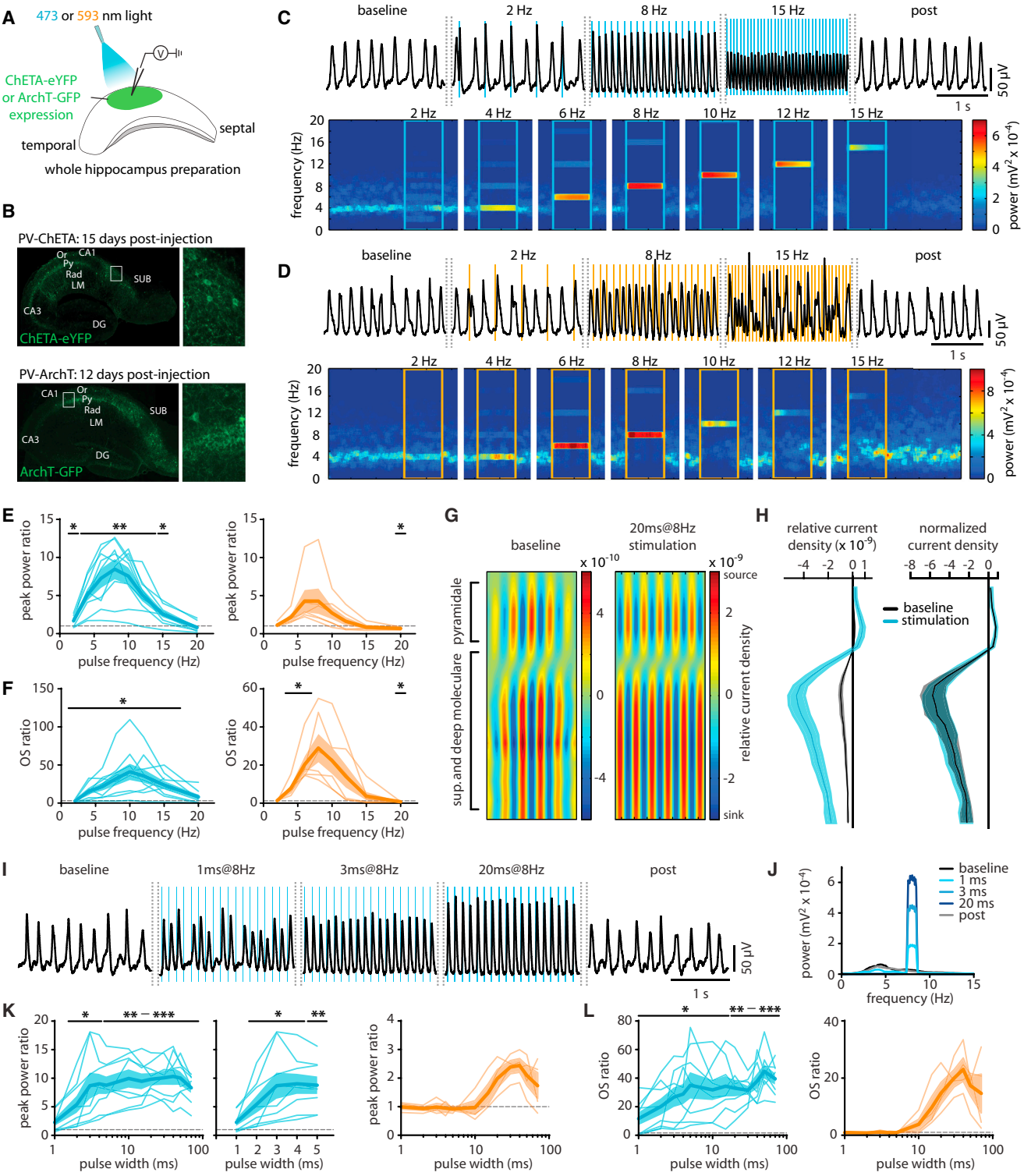

Figure 1. Optogenetic Stimulation of PV Interneurons Controls Theta Oscillations

(A) Cartoon representation of experimental setup.

(B) Transverse sections of intact hippocampus preparations showing ChETA-eYFP expression (top) and ArchT-GFP expression (bottom) in PvTom mice.

(C) Top: representative traces before, during, and after ChETA-expressing PV interneuron blue-light activation at different frequencies (20 ms pulse width). Bottom: Spectrograms of 30 s PV interneuron stimulations at 2 to 15 Hz (indicated by the blue boxes).

(legend continued on next page)

combining pharmacologically elicited theta in vitro and modeling have also underlined a potentially important role of O-LM interneurons in theta oscillations (Gillies et al., 2002; Gloveli et al., 2005). On the basis of their morphological and electrophysiological properties, both PV- and SOM-expressing interneurons thus seem ideally positioned to be essential in theta rhythm generation. However, a direct causal demonstration of their respective roles in theta generation in the hippocampus is still lacking.

Understanding which interneurons are directly involved in the intrinsic hippocampal theta rhythm and which ones are required to modulate the numerous inputs to intrinsic oscillators is a key aspect in understanding the mechanisms underlying hippocampal theta. In this study, we used optogenetics to selectively activate or inhibit PV and SOM interneurons in the complete hippocampus preparation in vitro (Goutagny et al., 2009). Intrinsic inhibitory-PC networks in this preparation are intact and generate spontaneous oscillations in the theta range in the absence of any input or pharmacological stimulation. This preparation thus allowed us to optogenetically stimulate or silence large portions of either PV or SOM interneuron networks during theta oscillations and determine which cell type is part of intrinsic hippocampal oscillators. Here, we show that phasic activation or silencing of PV interneurons drives intrinsic hippocampal oscillations optimally at 8 Hz. PV interneuron activation achieves this effect by strongly synchronizing PC firing. In addition, PV network phasic silencing disrupts endogenous theta rhythm. In contrast, activating or silencing SOM interneuron network had only a weak effect on intrinsic theta oscillations. However, optogenetically silencing SOM interneurons while simultaneously activating EC afferents revealed an important role of SOM cells in external input modulation. Our results thus place PV interneurons as key components of intrinsic hippocampal oscillators.

RESULTS

PV Interneurons Control Local Theta Rhythm

To study the respective contributions of PV and SOM interneurons to theta rhythm in the intact hippocampus preparation, the expression of either the activating opsin ChETA (Berndt et al., 2011) or the silencing opsin ArchT (Han et al., 2011) was driven by Cre-inducible adeno-associated viruses (AAVs) in the hippocampus of PV-Cre and SOM-Cre mice (Figures S1A and S2A). A high degree of specificity of ChETA expression was obtained in both cell populations in the SUB and dCA1 regions (Figure S1B). Light-activated photocurrent size (steady state), first action potential (AP) threshold, AP onset delay, and AP fidelity were measured by patch-clamp recordings in hippocampus slices in both dCA1 and SUB (Figures S1C–S1G). No significant difference was found between the dCA1 and SUB regions for PV or SOM interneurons, and therefore results from both subregions were pooled together. For all measured parameters, both cell types responded to blue light with similar efficiency (Figures S1D–S1G). ChETA-expressing interneurons recorded in patch-clamp were also submitted to theta-burst activation, which consisted of 20 to 70 ms square pulses of blue light repeated at 8 Hz for a duration of 30 s (Figure S1H). For field experiments, square light-pulse duration was set in order to trigger similar numbers of APs in PV and SOM cells (20 ms for PV, 50 ms for SOM, triggering on average two or three APs per pulse; Figure S1I). All cells exhibited stable firing over sweeps of 30 s stimulations, showing no increase in AP failure over time (Figures S1H–S1J). The properties of inhibitory post-synaptic potentials (IPSPs) elicited in PCs by stimulation of ChETA-expressing PV and SOM interneurons in hippocampal slices were also determined (Figures S1K–S1O). IPSP size was found to be largest for IPSPs elicited by PV cells in SUB (Figure S1M). A similarly high degree of specificity of ArchT expression was obtained in both cell populations in SUB and dCA1 regions (Figure S2B). No significant differences in the size of photocurrents or of membrane hyperpolarizations were found between both regions for the same interneuron type. Slightly larger hyperpolarizations (steady state) were measured in SOM interneurons compared with PV (Figures S2C and S2D), while photocurrent size (steady state) was similar (Figures S2C and S2E). ArchT-expressing interneurons also displayed stable photocurrents and hyperpolarizations in response to 30 s silencing protocols (Figure S2F). Therefore, the genetic targeting of ChETA or ArchT expression of PV and SOM cells allowed a very reliable, precise, and comparable control of their activity in the dCA1/SUB region of the hippocampus.

We first tested the role of PV interneurons in modulating the activity of the intrinsic hippocampal theta network. Spontaneously generated theta rhythm was recorded in dCA1/SUB region (baseline theta rhythm, average frequency 4.8 ± 0.2 Hz, n = 26), and then the light was delivered for periods of 30 s (Figures 1A and 1B). The absence of light-induced artifacts was verified before each experiment (Figure S3A). To determine whether

(D) Top: representative traces before, during, and after ArchT-expressing PV interneuron orange-light silencing at different frequencies (20 ms pulse width). Bottom: spectrograms of 30 s PV interneuron silencing at 2 to 15 Hz (orange boxes).
(E) Change in peak power (stimulation/baseline ratio) during activation of ChETA-expressing PV interneurons (left) or silencing of ArchT-expressing PV interneurons (right) at various frequencies (20 ms pulses; thin lines: individual preparations; thick line: average; shaded area: SEM).
(F) Change in OS (stimulation/baseline ratio) during PV interneuron activation (left) and silencing (right).
(G) Example CSD recorded during baseline oscillation (left) and ChETA-expressing PV interneuron activation (right) (20 ms pulses delivered at 8 Hz).
(H) Left: relative current density quantification before and during PV interneuron activation. Right: current density normalized to the peak. Mean ± SEM are plotted.
(I) Representative traces during simulation of ChETA-expressing PV interneurons with various lengths of blue-light pulses delivered at 8 Hz.
(J) Power spectrum of 8 Hz stimulation of PV interneurons with 1, 3, and 20 ms pulse widths.
(K) Left: change in peak power (stimulation/baseline ratio) for 8 Hz stimulation of ChETA-expressing PV interneurons (thin lines: individual preparations; thick line: average; shaded area: SEM). Middle: Same data emphasizing the linear increase in power of the oscillation for 1 to 3 ms pulses. The plateau of a 9-fold increase in peak power is reached as soon as 3 ms pulses occur. Right: change in peak power for 8 Hz silencing of ArchT-expressing PV interneurons.
(L) Change in OS for the same activation (left) and silencing (right) protocols.
*$p \leq 0.05$, **$p \leq 0.01$, and ***$p \leq 0.001$.

the field oscillations could be regulated by PV firing frequency, we rhythmically activated or silenced PV interneurons with light pulses delivered with a fixed duration (20 ms) at frequencies of 2 to 20 Hz. Rhythmic activation and silencing of PV interneurons both resulted in a robust pacing of the field oscillations (Figures 1C and 1D). Optogenetic activation and silencing at 2 Hz were unable to slow down the spontaneous oscillations (Figures 1C and 1D). At all frequencies within the theta range (4–10 Hz), rhythmic activation or silencing of PV interneurons overrode the baseline spontaneous theta oscillation independently of the original frequency of oscillation (Figures 1C and 1D). Activation of PV interneurons at frequencies above theta range could also pace the field oscillation (Figure 1C). Rhythmic silencing at higher frequencies was less efficient in pacing the oscillations and appeared to disrupt the baseline field activity (see example trace for 15 Hz, Figure 1D). Spectral analysis of the power of the field oscillation (Figures 1E, S4A, and S4B) and oscillation strength (OS; an index of rhythmicity, see Experimental Procedures; Figure 1F) revealed a significant effect of light-induced activation of PV interneurons on the field oscillation in the hippocampus. Interestingly, optogenetic activation of PV interneurons at 2 to 20 Hz showed a maximal increase in the peak power in response to 8 Hz stimulations (Figure 1E, left; 8.5 ± 1.3-fold increase, Holm's test, $t[8] = 5.7$, $p = 0.0034$) and a maximal increase in OS at 10 Hz (Figure 1F, left; 41.1 ± 10.6-fold increase, Holm's test, $t[8] = 3.8$, $p = 0.0218$). For rhythmic silencing of PV interneurons within the theta range, spectral analysis showed a trend toward an increase of the field oscillation power, although this effect did not reach significance (Figure 1E, right; Figures S4C and S4D). Rhythmic silencing of PV interneurons increased OS significantly for 4 and 6 Hz stimulations (Figure 1F, right; 4 Hz stimulation: 7.8 ± 1.6-fold increase, Holm's test, $t[5] = 4.4$, $p = 0.0481$; 6 Hz stimulation: 20.3 ± 4.3-fold increase, Holm's test, $t[5] = 4.4$, $p = 0.0471$). The peak increase in OS occurred for 8 Hz stimulation, although this effect did not reach significance (Figure 1F, right; 28.9 ± 7.4-fold increase, Holm's test, $t[5] = 3.8$, $p = 0.0660$). Interestingly, silencing PV interneurons at 20 Hz decreased both the power (Figure 1E, right; 0.7 ± 0.1, Holm's test, $t[5] = 4.6$, $p = 0.0455$) and rhythmicity of the field oscillation (Figure 1F, right; 0.7 ± 0.1, Holm's test, $t[5] = 4.5$, $p = 0.0495$). Control experiments consisting of light stimulations to yellow fluorescent protein (YFP) transduced alone had no effect on theta rhythm (Figures S3B–S3D). Thus, synchronizing the activity of a large population of PV interneurons at theta frequency robustly entrains the hippocampal network and regulates the frequency, power, and rhythmicity of intrinsically generated oscillations. PV interneurons receive rhythmic inputs from septal GABAergic neurons, which have been suggested to be important in the generation of hippocampal theta in vivo (Wulff et al., 2009). Experiments using rhythmic silencing of PV interneurons mimic GABAergic septal inputs and show that synchronizing PV interneurons through inhibitory inputs is an important mechanism in hippocampal theta generation. Interestingly, synchronizing the PV interneuron population through either activation or silencing entrains hippocampal network optimally at 6 to 10 Hz, suggesting that PV interneurons interact optimally with PCs at frequencies within the in vivo theta range.

In order to establish whether the site of phase reversal remained constant when rhythmically activating ChETA-expressing PV interneurons, we performed a current source density (CSD) analysis (Figures 1G and 1H). Current density was significantly different between baseline and PV interneuron activation, as expected from the strong increase in the power of the field oscillation when activating PV interneurons (Figure 1H, left; two-way repeated-measures ANOVA, PV stimulation × depth interaction, $F[11, 154] = 27.4$, $p < 0.0001$). Yet normalized current density displayed very similar profiles, suggesting a similar site of phase reversal during PV interneuron activation (Figure 1H, right; two-way repeated-measures ANOVA, PV stimulation × depth interaction, $F[11, 154] = 0.04$, $p > 0.9999$). Thus, the changes in the field oscillation generated by PV interneuron activation arose locally in the dCA1/SUB hippocampal network and did not modify phase reversal.

ChETA-expressing PV interneurons were stimulated at 8 Hz with various light-pulse durations in order to increase the number of AP per stimulation and progressively recruit a larger portion of the PV network (Figure 1I). We determined whether increased recruitment of PV interneurons increased the power of the field oscillation. Light activation with pulses as short as 1 ms (which elicited an AP in only a portion of the interneurons) (Figure S1E) partly drove the ongoing oscillations (Figures 1I and 1J), while longer pulses (2–70 ms) resulted in the generation of a robust 8 Hz oscillation (Figures 1I–1K). The maximum increase in peak power was reached using 40 ms pulses (Figure 1K, left; 10.3 ± 1.5-fold increase, Holm's test, $t[7] = 6.2$, $p = 0.0035$). The middle part of Figure 1K is an inset showing the linear increase in peak power for stimulations between 1 and 3 ms, likely reflecting the progressive recruitment of the PV network. OS was also strongly increased, reaching a maximum for 50 ms pulses (Figure 1L, left; 44.7 ± 5.0-fold increase, Holm's test, $p = 0.0005$). Rhythmic silencing of ArchT-expressing PV interneurons showed a clear trend toward an increase in power and rhythmicity of the field oscillation, although this effect did not reach significance (Figure 1K, right, and Figure 1L, right). The change in power or OS appeared only for orange-light pulses larger than 10 ms, suggesting that the mechanism underlying this effect seems to require the silencing of a large portion of PV interneuron network.

Last, using sustained light-induced activation, we determined whether overall increases in PV neuronal activity could drive the network oscillations near theta frequency (Figures 2A–2C). When a continuous 10 s activating light pulse was delivered to PV interneurons, the frequency of spontaneous oscillations shifted to faster frequencies accompanied on average by a decrease in power of the oscillations (Figures 2A–2C). For all recorded preparations, the average frequency of theta increased from 4.8 ± 0.4 to 7.9 ± 0.4 Hz ($n = 9$, t test, $t[16] = 5.7$, $p < 0.0001$) during continuous 10 s light pulses (Figure 2B). We found that continuous stimulation of the PV interneuron network induced a significant increase in frequency (Figure 2C; activation over baseline ratio [stim/base ratio] = 1.71 ± 0.16, one-sample t test, $t[8] = 4.5$, $p = 0.0020$). In line with the strong increase in the frequency of oscillation, continuous stimulation of PV network induced a decrease in power at baseline dominant frequency (BDF) (stim/base ratio = 0.19 ± 0.07, one-sample t test, $t[8] = 11.2$, $p < 0.0001$), peak power (stim/base ratio = 0.62 ± 0.11, one-sample

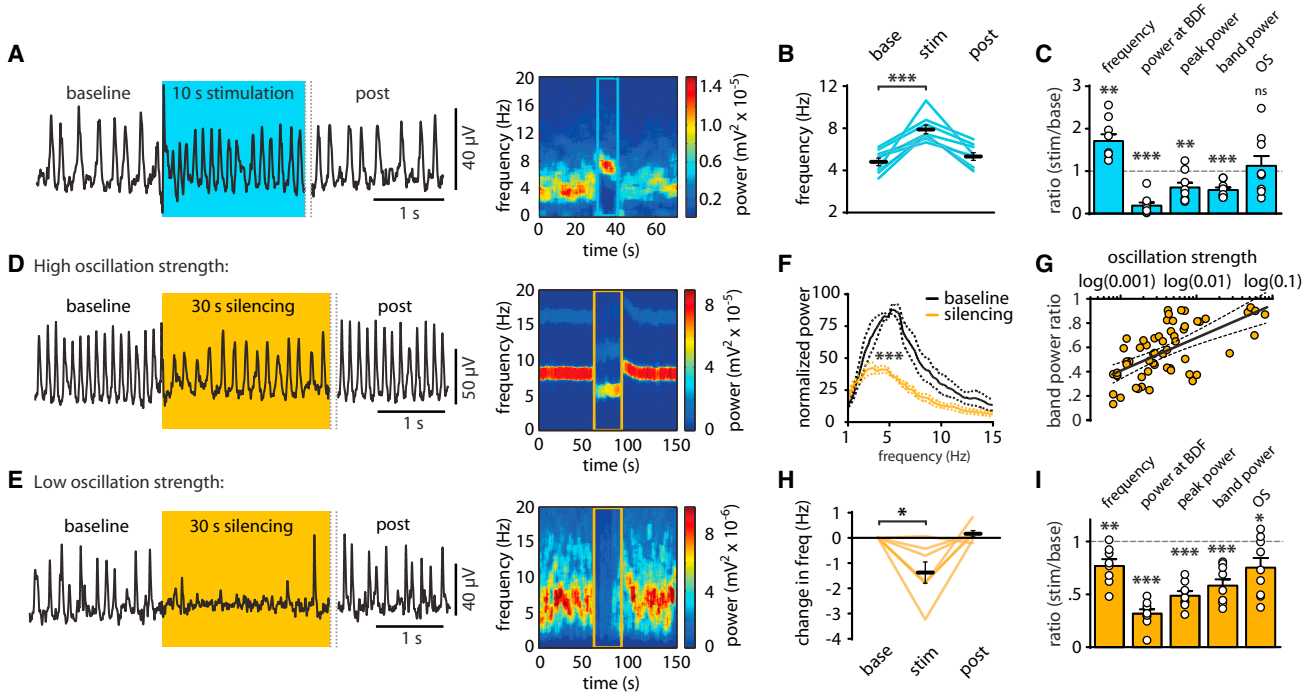

Figure 2. Tonic Activation of PV Interneurons Triggers Theta, and Tonic Silencing Disrupts the Endogenous Rhythm

(A) Representative traces recorded in the intact hippocampus before, during, and after ChETA-expressing PV interneuron 10 s continuous activation and spectrogram for the same stimulation.

(B) Continuous activation of PV interneurons increased the spontaneous theta oscillations frequency from 4.8 ± 0.4 to 7.9 ± 0.4 Hz (lines: individual preparations; bars: mean ± SEM).

(C) Quantification of the effect of a 10 s tonic stimulation of ChETA-expressing PV interneurons (stimulation/baseline ratio) on frequency, peak power at the BDF, peak power, band power, and OS of the field oscillation (mean ± SEM).

(D) Example trace (left) and spectrogram (right) for a 30 s silencing of ArchT-expressing PV interneurons (indicated by the orange box) in which both frequency and power of theta oscillations are strongly reduced.

(E) Second example of PV interneuron silencing in which theta activity during PV interneuron silencing is completely disrupted.

(F) Averaged power spectrums for ArchT-expressing PV interneuron silencing, showing a strong decrease in power of the oscillation (dotted lines: SEM). For each hippocampus preparation, two to nine recordings were averaged and normalized to the peak of the baseline power spectrum.

(G) Correlation between the extent of change in power while silencing PV interneurons (band power, 0.5–25 Hz) and OS. Solid line is the linear fit to the data (dotted lines indicate 95% confidence interval).

(H) The decrease in theta frequency when silencing PV interneurons was on average −1.4 ± 0.4 Hz (lines: individual preparations; bars: mean ± SEM).

(I) Quantification of the effect of a 30 s tonic silencing of ArchT-expressing PV interneurons (stimulation/baseline ratio) on frequency, peak power at the BDF, peak power, band power, and OS of the field oscillation (mean ± SEM).

*p ≤ 0.05, **p ≤ 0.01, and ***p ≤ 0.001.

t test, t[8] = 3.4, p = 0.0088), and band power (stim/base ratio = 0.56 ± 0.06, one-sample t test, t[8] = 7.1, p < 0.0001). Sustained 10 s stimulation of PV interneuron network induced no change in OS (Figure 2C). These results suggest that increasing the overall excitability of PV interneurons shifts the network rhythm to a frequency similar to that of in vivo theta.

Collectively, these data using rhythmic activation or silencing of PV interneurons as well as sustained activation demonstrate that PV interneurons regulate the power and frequency of intrinsic hippocampus oscillators within the range of in vivo theta oscillations.

PV Interneuron Silencing Disrupts Local Theta

We next tested the effect of continuously silencing ArchT-expressing PV interneurons. Spontaneous theta oscillations were recorded in the dCA1/SUB region when the CA3 region was not active (in order to avoid confounding oscillatory inputs; see Supplemental Information). Light-induced silencing of the ArchT-expressing PV cells resulted in a strong decrease in the frequency and power of the ongoing theta activity (Figures 2D and 2F; averaged power spectrum, n = 5, two-way repeated-measures ANOVA, PV stimulation × frequency interaction, F[196, 1,568] = 3.7, p < 0.0001). In some cases (23.7% of all recordings), theta oscillations were completely abolished during the optogenetic silencing (Figure 2E). The decrease in frequency and power remained stable over the 30 s period of silencing, and the spontaneous theta activity resumed when the light was turned off. We noticed that the power of theta was reduced to different extents when silencing PV interneurons. Interestingly, the difference in power reduction between experiments during PV silencing was significantly correlated with the baseline OS, a measure of network rhythmicity and synchronization

(Figure 2G; linear regression, $R^2 = 0.3847$, $p < 0.0001$). Because we have previously shown that theta in dCA1/SUB region is generated by the synchronization of loosely connected oscillators across the septo-temporal axis of the hippocampus (Goutagny et al., 2009), this suggests that the PV silencing is most effective when the target network contains fewer synchronized oscillators. When the remaining theta activity during PV interneuron silencing was considered large enough to analyze the frequency of oscillations (peak power baseline/stimulation ratio > 0.3, 71.4% of all recordings), PV silencing decreased the frequency of the field oscillation by 1.4 ± 0.4 Hz (Figure 2H; one-sample t test, t[6] = 3.3, p = 0.0167). Altogether, silencing PV interneurons induced a significant decrease in frequency (Figure 2I; stim/base ratio = 0.77 ± 0.06, one-sample t test, t[7] = 3.7, p = 0.0074), power at BDF (stim/base ratio = 0.32 ± 0.04, one-sample t test, t[8] = 11.2, p < 0.0001), peak power (stim/base ratio = 0.49 ± 0.04, one-sample t test, t[8] = 13.0, p < 0.0001), band power (stim/base ratio = 0.58 ± 0.06, one-sample t test, t[8] = 7.1, p = 0.0001), and OS (stim/base ratio = 0.75 ± 0.09, one-sample t test, t[8] = 2.7, p = 0.0265). Therefore, silencing PV interneuron network can produce extensive reductions in intrinsic hippocampal theta generation, further suggesting that PV-PC connectivity is necessary to intrinsic theta rhythm generation.

PV Interneurons Phase PC Firing

To determine the mechanisms underlying the control of theta generation by PV interneurons, we investigated the modulation of PC spike timing in relation to theta oscillations. Local field potential (LFP) and extracellular multiunit activity (MUA) were simultaneously recorded during optogenetic activation or silencing of PV interneurons at different frequencies in the intact hippocampus preparation (Figures 3A and 3B). We first examined the delay between putative PC firing and the onset of the light pulses during activation and silencing of PV interneurons (Figure 3C). MUA suspected to be from PV interneurons were eliminated from the analysis (see example in Figure S3E). When activating PV interneurons, the peak of putative PCs discharge occurred on average 16 to 18 ms after blue-light onset (Figure 3C). In contrast, when silencing PV interneurons, the average peak of putative PC discharge was 44 ms after orange-light onset (corresponding to 24 ms after orange-light offset), suggesting that PCs fire in rebound to PV interneuron firing. Light-induced activation of PV interneurons increased the number of spikes per theta cycle of putative PCs significantly for 2 Hz stimulations (Figures 3B and 3D; +1.2 ± 0.6 APs per cycle, Holm's test, t[4] = 8.9, p = 0.0054). The peak increase in the number of APs per cycle occurred for 4 Hz activation, although this effect did not reach significance (Figures 3B and 3D; +2.4 ± 0.6 APs per cycle, Holm's test, t[4] = 3.8, p = 0.0922). Circular variance, which reflects the distribution of PC units around the peak of theta cycles, decreased during PV interneuron activation (Figures 3B and 3E; 8 Hz activation: −0.58 ± 0.09, Holm's test, t[4] = 6.5, p = 0.0176). Last, in accordance with the increase in spikes per cycles and the decrease in circular variance, vector length tended to increase during optogenetic stimulation of PV interneurons, because of the MUA being more locked to the field oscillations (Figure 3F). Overall, putative PCs increased their firing rate and their synchronization with 4 to 10 Hz stimulations, corresponding to the maximum increase in peak power and OS demonstrated for theta field recordings in Figures 1E and 1F. In contrast, no significant differences in PC MUA were observed following ArchT-expressing PV interneuron rhythmic silencing (Figures 3D–3F). As shown on the raster plots (Figure 3G), continuous silencing of PV interneurons led to increased variability in the timing of PC units relative to spontaneous oscillations. During PV interneuron silencing, the extent of the power decrease was correlated with the decrease in the number of units per theta cycle (Figure 3H; linear regression, $R^2 = 0.2190$, $p = 0.0018$), and similarly, larger decreases in peak power correlated with an increased variability of PC spiking relatively to theta peak (Figure 3I; linear regression, $R^2 = 0.1290$, $p = 0.0153$). Thus, strong decreases in power during PV interneuron silencing can be explained by less PC spiking and increased spike-timing variability during each theta cycle. Our results provide further evidence of the unique capacity of PV interneurons to efficiently synchronize PC activity in the dCA1/SUB region of the hippocampus.

SOM Interneurons Participate in Intrinsic Theta Generation

We next determined the implication of SOM-positive interneurons in modulating the activity of intrinsic theta oscillators in the hippocampus. Light stimulations were applied for periods of 30 s to activate or silence ChETA- and ArchT-expressing SOM interneurons (Figures 4A and 4G). The baseline frequency of spontaneous theta oscillations was similar in PV and SOM intact hippocampus preparations (PV: 4.8 ± 0.2 Hz, n = 26; SOM: 4.7 ± 0.2 Hz, n = 38; t test, t[62] = 0.6, p = 0.5433). Activation of SOM interneurons with light pulses of fixed duration (50 ms) delivered from 2 to 20 Hz did not significantly affect the power or OS of the ongoing oscillation (Figures 4B–4D). Yet when changes in power and oscillation strength were expressed as a function of the frequency of stimulation over baseline frequency ratio (Fstim/Fbase) (Figures 4E and 4F), a significant increase in OS was observed (binned data: bin size = 0.4, Fstim/Fbase = 1.0, 1.5 ± 0.2-fold increase in OS, t test, t[7] = 3.1, p = 0.0179). Thus, SOM interneurons can significantly pace the oscillation when activated at a frequency close to the baseline rhythm. We next measured the consequences of silencing SOM interneurons on spontaneous theta oscillations (Figures 4G–4J). Silencing SOM interneurons had an overall small effect on the oscillations (Figures 4H and 4I; averaged power spectrum, n = 11, two-way repeated-measures ANOVA, SOM stimulation × frequency interaction, F[196, 3,528] = 1.2, p = 0.0640). On average, a small but significant change in some parameters of the field oscillation could be measured (Figure 4J). Indeed, silencing SOM interneurons slightly decreased the frequency of oscillations (stim/base ratio = 0.91 ± 0.03, one-sample t test, t[14] = 2.9, p = 0.0115), power at BDF (stim/base ratio = 0.77 ± 0.07, one-sample t test, t[14] = 3.3, p = 0.0054), and band power (stim/base ratio = 0.89 ± 0.05, one-sample t test, t[14] = 2.2, p = 0.0476). The peak power and OS of the ongoing field were unaffected by SOM interneuron silencing (Figure 4J). When compared with continuous silencing of PV interneurons, SOM interneuron silencing induced significantly weaker decreases in frequency, power at BDF, peak power, and band power of the ongoing oscillations (Figures S4E–S4I). Last, we analyzed the

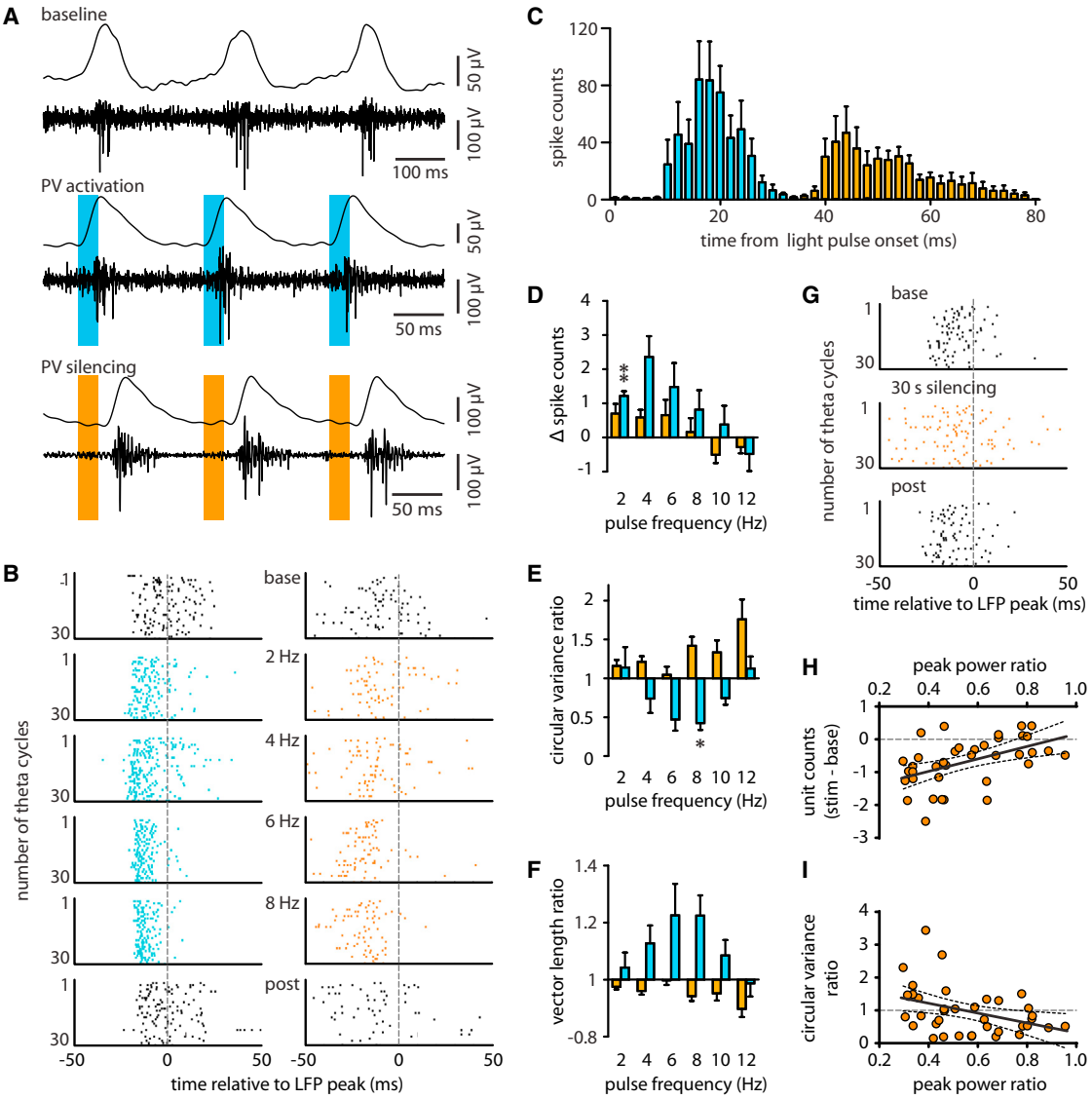

Figure 3. PV Interneuron Optogenetic Manipulation Modifies PC Firing

(A) Example of LFPs and MUA for baseline (top), ChETA-expressing PV interneuron activation (middle), and ArchT-expressing PV interneuron phasic silencing (bottom).

(B) Raster plots showing putative PC activity during phasic activation (left) or silencing (right) of PV interneurons at different frequencies. The spiking of putative PCs is shown for 30 consecutive theta cycles, aligned to the peak (0 ms, dotted line).

(C) Spike histogram showing MUA relative to the onset of light pulses in the case of ChETA-expressing PV interneuron activation (blue) and ArchT-expressing PV interneuron silencing (orange). Error bars are SEM.

(D) Difference in the number of spikes per theta cycle between stimulation and baseline during activation (ChETA, blue) or silencing (ArchT, orange) of PV interneurons at theta frequencies (pulse width 20 ms; mean ± SEM).

(E) Change in circular variance (stimulation/baseline ratio, expressed as the change relative to 1).

(F) Change in vector length (stimulation/baseline, expressed as the change relative to 1).

(G) Raster plots showing putative PC activity during 30 s continuous silencing of ArchT-expressing PV interneurons.

(H) The decrease in theta peak power during PV interneuron silencing was correlated to the difference in number of spikes per theta cycle. The solid line is the linear fit to the data (dotted lines indicate 95% confidence interval).

(I) The decrease in theta peak power was also correlated with an increase in circular variance ratio during PV interneuron silencing.

*$p \leq 0.05$ and **$p \leq 0.01$.

modulation of PC discharge in relation to theta oscillation during SOM interneuron optogenetic manipulation. SOM interneuron activation (Figures 4K and 4L) or silencing (data not shown) did not modify the number of putative PC spikes per theta cycle, the circular variance of PC firing, or the phase locking of PCs to the ongoing field oscillation. Overall, in contrast to the clear

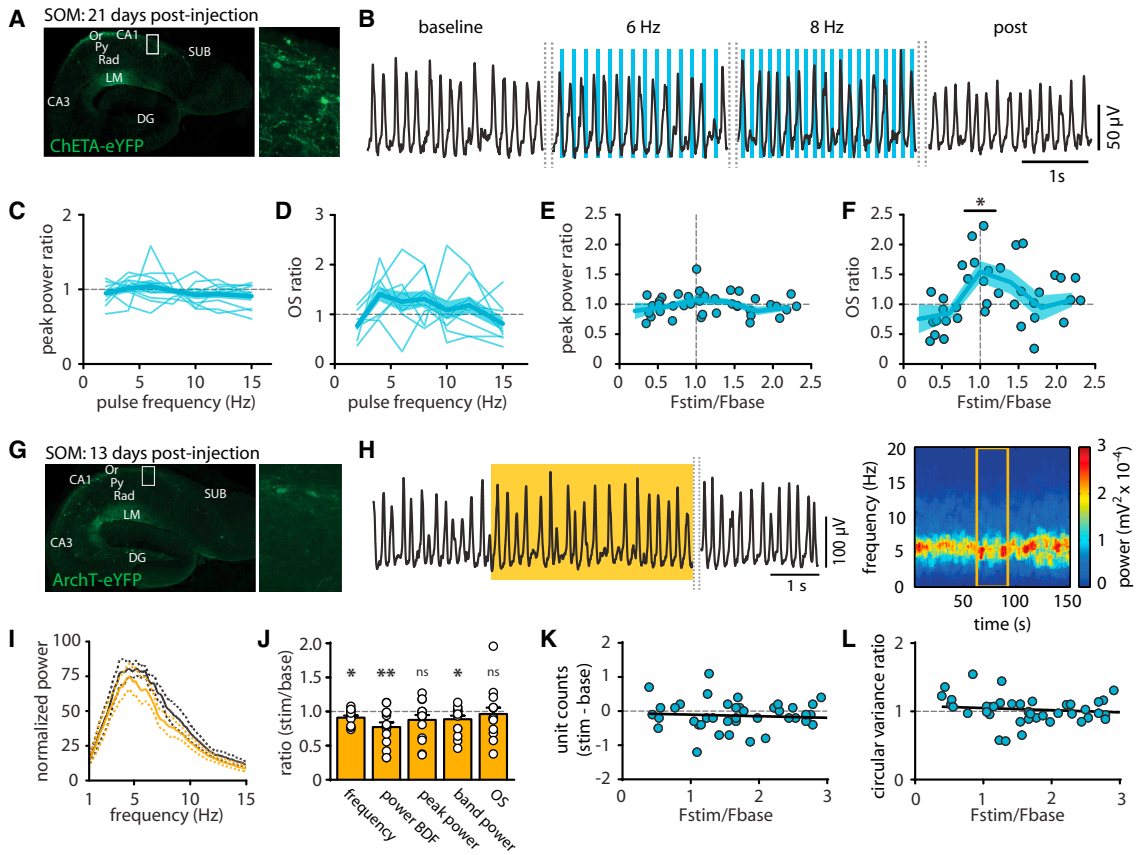

Figure 4. SOM Interneurons Weakly Participate in Intrinsic Theta Modulation

(A) Transverse sections of an intact hippocampus preparation showing ChETA-eYFP expression in SomTom mice.

(B) Example traces showing 6 and 8 Hz activation of ChETA-expressing SOM interneurons (50 ms pulse width).

(C) Phasic SOM interneuron activation at various frequencies within theta range had no significant effect on peak power (thin lines: individual preparations; thick line: average; shaded area: SEM).

(D) For the same activation protocols, oscillations showed no change in OS.

(E) Change in power during SOM interneuron activation expressed as a function of the frequency of stimulation/ baseline theta frequency (thick line: mean of the binned data; six bins, bin size = 0.4; shaded area: SEM). SOM interneuron activation had no effect on power.

(F) OS was increased by SOM interneuron activation for Fstim/Fbase values close to 1.0.

(G) Transverse sections of an intact hippocampus preparation showing ArchT-GFP expression in SomTom mice.

(H) Example trace (left) and spectrogram (right) for a 30 s continuous silencing of ArchT-expressing SOM interneurons (orange box).

(I) Averaged power spectrum for SOM interneuron silencing (dotted lines: SEM). For each hippocampus preparation, one to six recordings were averaged and normalized to the peak of the baseline power spectrum.

(J) Quantification of the effect of a 30 s silencing of SOM interneurons (stimulation/baseline ratio) on frequency, peak power at the BDF, peak power, band power, and OS of the field oscillation (mean ± SEM).

(K) Difference in the number of spikes per theta cycle between stimulation and baseline during SOM interneuron activation, expressed as a function of Fstim/ Fbase. Solid line is the linear fit to the data.

(L) Change in circular variance (stimulation/baseline ratio) as a function of Fstim/Fbase.

*$p \leq 0.05$ and **$p \leq 0.01$.

role of PV interneurons, SOM interneurons do not appear to play a prominent role in the generation of intrinsic theta rhythm in the hippocampus.

SOM Interneurons and EC Inputs Interact to Modulate Intrinsic Theta

Although SOM interneurons played a minor role in intrinsic theta generation, we next determined whether they could significantly modulate external input to the hippocampus. The EC sends highly topographically organized projections to the hippocampal circuitry, contacting directly SUB and dCA1 sub-regions through the temporoammonic (TA) pathway (van Strien et al., 2009). In CA1, TA pathway projections synapse on distal dendrites of PCs in stratum lacunosum-moleculare, which is also the target of SOM-positive OLM interneurons on PCs. SOM interneurons have been shown to regulate EC inputs onto CA1 PCs (Leão et al., 2012; Lovett-Barron et al., 2014). We thus sought to determine if SOM interneurons were involved in modulating TA pathway inputs. Therefore, we designed optogenetic experiments to concomitantly activate the TA pathway and

silence SOM interneurons during theta oscillations. Expression of ChETA in the TA pathway was obtained using AAV vector driving ChETA expression under the control of the CamKIIα promoter, and similarly to our previous experiments, SOM cells were silenced using ArchT (Figure 5A). Accordingly, TA fibers strongly expressed ChETA in the hippocampus in dCA1 (stratum lacunosum-moleculare) and in the SUB (Figure 5A). Considering the physical proximity of the EC and hippocampus within the mouse brain, we confirmed the complete absence of leakage of ChETA expression in the hippocampus after AAV-CamKIIα-ChETA injections in the EC (n = 4, data not shown). We first performed patch-clamp experiments in hippocampus slices from mice injected only in the EC with AAV-CamKIIα-ChETA, in order to quantify the impact of activating TA pathway fibers on PCs in dCA1 and SUB (Figure S5). In both dCA1 and SUB PCs, ChETA-expressing TA pathway activation resulted in the expected biphasic post-synaptic response, consisting of a direct monosynaptic excitation by TA, followed by feedforward inhibition (Empson and Heinemann, 1995) (Figure S5A). Interestingly, the post-synaptic depolarization was stronger in SUB PCs relative to dCA1 (Figure S5B). As a consequence, SUB PCs could be driven by activating ChETA-expressing TA pathway inputs in hippocampal slices (Figures S5D and S5E). We next quantified the impact of rhythmically activating ChETA-expressing TA pathway in the intact hippocampus preparation (Figure 5A). Pulses of 20 ms duration blue light were delivered in 1 Hz steps at frequencies within the theta range (2–10 Hz). Activation of ChETA-expressing TA fibers was able to drive the spontaneous field oscillations over a restricted range of frequencies in comparison with PV interneuron activation (Figure 5B). Increases in the power of the oscillation were observed over the different frequencies (Figure 5C). This increase in power was significant only for stimulations at 4 Hz (2.3 ± 0.2-fold increase, Holm's test, $t[5] = 5.6$, $p = 0.0232$). TA pathway fiber activation in hippocampus also tended to increase the OS with no clear preference for any frequency within the range of stimulations (Figure 5D). The changes in power and OS when activating TA pathway fibers were thus expressed as a function of Fstim/Fbase in order to account for the ratio between frequencies of stimulation and baseline oscillation (Figures 5E and 5F). The activation of TA pathway fibers increased the power of the oscillations when the frequency of activation was delivered near the frequency of baseline oscillations (Figure 5E; binned data: bin size = 0.3; Fstim/Fbase = 1.0: 2.1 ± 0.3-fold increase, Holm's test, $t[8] = 4.2$, $p = 0.0215$; Fstim/Fbase = 1.3: 2.8 ± 0.3-fold increase, Holm's test, $t[9] = 6.0$, $p = 0.0016$; Fstim/Fbase = 1.6: 3.0 ± 0.5-fold increase, Holm's test, $t[7] = 3.9$, $p = 0.0356$). OS was also significantly increased by ChETA-expressing EC fiber activation (Figure 5F; bin size = 0.3; Fstim/Fbase = 1.3: 14.3 ± 2.5-fold increase, Holm's test, $t[9] = 5.4$, $p = 0.0036$; Fstim/Fbase = 1.6: 17.7 ± 4.2-fold increase, Holm's test, $t[7] = 4.0$, $p = 0.0352$). When the activation over baseline frequency ratio was close to 1.0, OS showed a clear trends toward an increase, although the effect did not reach significance (Fstim/Fbase = 1.0: 6.4 ± 1.6-fold increase, Holm's test, $t[8] = 3.4$, $p = 0.0559$). Thus, driving the EC inputs does not override the baseline oscillations, as observed for PV interneuron activation, but rather can entrain the hippocampal oscillators at a frequency close or slightly above the spontaneous frequency of the system.

We next repeated the TA fiber activation protocols while simultaneously silencing SOM interneurons (Figures 5G and 5H; see Experimental Procedures). Interestingly, the increase in power observed during activation of ChETA-expressing TA fibers was strongly attenuated when ArchT-expressing SOM interneurons were simultaneously silenced (Figure 5G). The effect of activating TA fibers on OS was also diminished, yet remained significant for Fstim/Fbase ratios close to 1.0 (Figure 5H; bin size = 0.3, 5.8 ± 1.2-fold increase, Holm's test, $t[10] = 4.0$, $p = 0.0205$) and almost reached significance for Fstim/Fbase ratios close to 1.3 (12.0 ± 3.2-fold increase, Holm's test, $t[9] = 3.5$, $p = 0.0502$). We compared the effect of TA pathway activation alone with simultaneous TA activation and SOM interneuron silencing (Figures 5I and 5J). For the frequency ratio at which the increase in power was maximal for TA fiber stimulation, simultaneously silencing SOM interneurons significantly attenuated this effect (Figure 5I; Fstim/Fbase = 1.6; TA activation: 3.0 ± 0.5-fold increase; TA activation and SOM silencing: 1.2 ± 0.2-fold increase; t test, $t[16] = 3.7$, $p = 0.0020$). The same result was found for OS (Figure 5J; Fstim/Fbase = 1.6; TA activation: 17.7 ± 4.2-fold increase; TA activation and SOM silencing: 3.4 ± 2.1-fold increase, t test, $t[16] = 3.3$, $p = 0.0046$). SOM interneuron silencing thus significantly dampens the effect of TA pathway activation on hippocampal intrinsic theta rhythm.

Last, we analyzed the modulation of PC spike timing in relation to theta oscillation during the activation of TA fibers with or without simultaneous SOM interneuron silencing (Figures 5K and 5L). On average, the increase in power due to TA pathway fiber activation was not accompanied by a change in the number of putative PC spikes per theta cycle (Figure 5K, black; difference in spike count between baseline and stimulation = 0.09 ± 0.12, one-sample t test, $t[25] = 0.7$, $p = 0.4726$). Interestingly, when SOM interneurons were silenced simultaneously to TA pathway fiber activation, the number of PC spikes in response to TA pathway activation significantly decreased (Figure 5K, orange; difference in spike count between baseline and stimulation = −0.31 ± 0.07, one-sample t test, $t[20] = 4.2$, $p = 0.0004$). Thus, PC discharge was modified during simultaneous SOM silencing and TA fiber activation compared with TA activation alone (Figure 5K; t test, $t[45] = 2.6$, $p = 0.0059$). Finally, the timing of PC spiking relative to the onset of blue-light stimulation of TA pathway fibers was analyzed. When TA pathway fibers were activated alone, the peak of putative PC firing occurred on average 36 ms after light onset, but occurred 42 ms after light onset when SOM cells were concomitantly silenced. SOM interneuron silencing thus delayed putative PC firing in response to TA pathway activation by 6 ms, and significantly altered PC spike distribution (Figure 5L; TA activation alone, n = 5, TA activation and SOM silencing, n = 6, two-way repeated-measures ANOVA, SOM stimulation × time from light onset interaction, $F[19, 171] = 2.2$, $p = 0.0038$). These results show that SOM interneurons can modulate the strength of the TA pathway input on dCA1/SUB PC firing.

Overall, these results demonstrate that optogenetic activation of excitatory EC projections to dCA1/SUB can increase theta power and rhythmicity. Interestingly, simultaneously silencing SOM interneurons diminished the effect of EC fiber activation on hippocampal intrinsic oscillators and altered the spiking

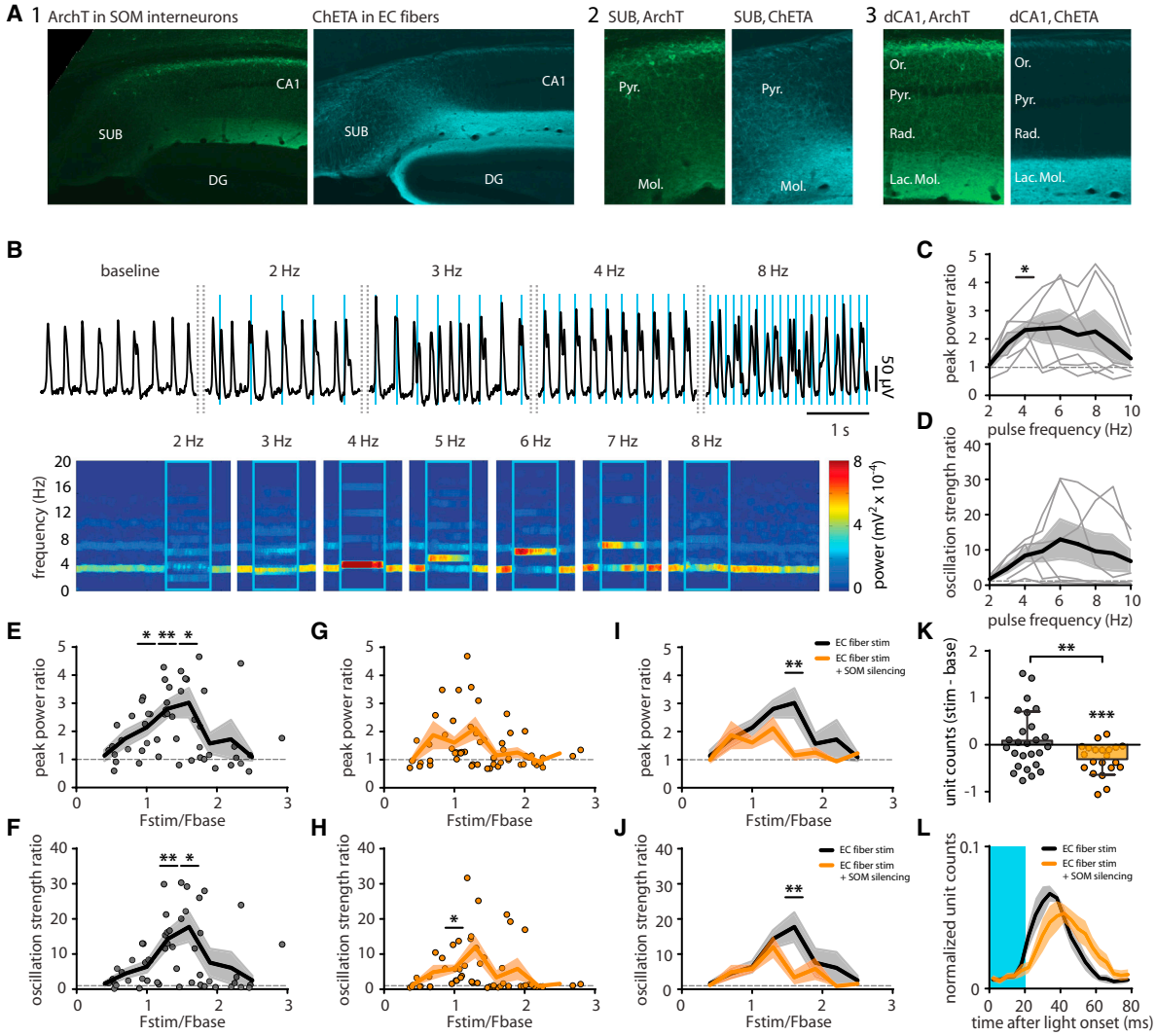

Figure 5. SOM Interneurons Modulate EC Inputs

(A) (1) Cre-dependent ArchT expression in SOM interneurons (left, green) and ChETA expression in CamKII-expressing neurons from the TA pathway (right, cyan) in the dCA1/SUB region of SomTom mice. (2) Enlargement showing ArchT-expressing SOM interneurons and ChETA-expressing TA pathway fibers in the SUB. (3) Enlargement in dCA1.

(B) Top: representative traces before, during, and after ChETA-expressing TA pathway activation at different frequencies (20 ms pulse width). Bottom: spectrograms of 30 s TA pathway activation at 2 to 8 Hz (blue boxes).

(C) Change in peak power of the oscillation (stimulation/baseline ratio) as a function of the frequency of ChETA-expressing TA pathway activation (thin lines: individual preparations; thick line: average; shaded area: SEM).

(D) Change in OS (stimulation/baseline ratio).

(E) Change in peak power during TA pathway activation as a function of the frequency of stimulation/baseline frequency ratio (Fstim/Fbase). The thick line is the mean of the binned data; eight bins were used (bin size = 0.3 except for the last bin, which groups detuning values ranging from 2.35 to 4.10); shaded area: SEM.

(F) Change in OS during TA pathway activation. Bin number and size are the same as in (E).

(G) Change in peak power during simultaneous TA pathway activation and SOM interneuron silencing. See Figure S5 for patch-clamp controls of the effect of orange-light on ChETA and blue-light on ArchT. Bin number and size are the same as in (E).

(H) Change in OS. Bin number and size are the same as in (E).

(I) Change in peak power compared between TA pathway activation alone (black) and with simultaneous SOM interneuron silencing (orange).

(J) Change in OS.

(K) Difference in the number of spikes per theta cycle between stimulation and baseline, for TA pathway activation without (black) or with (orange) SOM interneuron silencing (mean ± SEM). This analysis was restricted to recordings in which Fbase/Fstim was between 0.85 and 1.75, corresponding to frequency ratios at which TA pathway activation significantly increased theta power (bins centered on 1.0, 1.3, and 1.6, see E).

(L) Stimulation triggered spike histogram showing the spiking of putative PCs relative to blue-light onset (shaded area: SEM); analysis performed on the same recordings as in (K). Recordings from the same hippocampus preparation were averaged (one to six recordings per preparation).

*$p \leq 0.05$, **$p \leq 0.01$, and ***$p < 0.001$.

behavior of PCs. EC inputs and SOM interneurons thus seem to be able to interact in order to modulate the activity of intrinsic hippocampal theta networks. These results suggest that SOM interneurons could be implicated in a disinhibitory mechanism regulating PC firing.

DISCUSSION

Hippocampal interneurons receive both internal and external input and are widely believed to be a central component to theta generation. The goal here was to determine the causal role of two interneuron populations, PV and SOM interneurons, in the generation of theta by intrinsic hippocampus oscillators. We used an intact hippocampus preparation in which all intrinsic excitatory-inhibitory connections are preserved, while external inputs are removed (medial septum, EC, contralateral hippocampus). In addition, the intact hippocampus offers the opportunity to optogenetically control very large cellular networks. This combination of techniques thus offers a novel approach to dissect the networks necessary for generation of intrinsic theta oscillations in the hippocampus. It has indeed been clearly demonstrated that the hippocampus contains intrinsic theta generators (Goutagny et al., 2009; Gu et al., 2013). What cell types and cellular mechanisms contribute to theta oscillators remains unclear. Both in vitro slice work and in vivo studies provide approaches that help answer some of the questions but also have important limitations. Indeed, in vitro slice studies bring important information on cellular mechanisms but dramatically disrupt the hippocampus network organization. In comparison, in vivo studies have now clearly demonstrated the phase locking of various hippocampal interneurons to theta rhythm (Klausberger and Somogyi, 2008; Varga et al., 2012), yet the causal contribution of interneuron subtypes to intrinsic hippocampus theta generation remains unclear. Here we used an approach whereby external oscillators were eliminated to concentrate on which interneurons appeared to be central for intrinsic theta generation.

PV and PC Networks Are the Basic Units of dCA1/SUB Intrinsic Oscillators

Our results using phasic optogenetic activation showed that increasing PV cell excitability increased the power, whereas the frequency of PV cell firing directly set the frequency of the field oscillation. Interestingly, the peak increase in field power was obtained using optogenetic stimulation at 8 Hz, indicating that the network of PV interneurons and PCs interacts optimally at a theta-relevant frequency. This finding is also corroborated by the optogenetic tonic stimulations of the PV interneurons, which resulted in shifting the baseline oscillation frequency up to 8 Hz, further suggesting that the inhibitory-excitatory network naturally oscillates at theta frequency. PV interneuron network generates theta by strongly synchronizing putative PCs (i.e., increasing the number of spikes and/or decreasing the jitter of these units during each theta cycle). By tightly controlling the discharge timing of large PC networks, PV interneurons are, as suspected, powerful coordinators of hippocampal network activity and constitute one of the basic components of hippocampal intrinsic oscillators (Cobb et al., 1995). Phasic optogenetic silencing of PV interneurons further confirmed the instrumental role of PV interneurons in intrinsic theta generation. Medial septum inhibitory inputs to the hippocampus have been shown to synapse preferentially on GABAergic interneurons (Freund and Antal, 1988), and phasic inhibitory inputs on PV-expressing interneurons have been suggested as an important mechanism contributing to hippocampal rhythms (Wulff et al., 2009). Our results further support the idea that phasic inhibition onto PV interneurons appears as a prominent theta generation component, in line with a wealth of studies emphasizing the role of medial septum GABAergic projections in hippocampal theta generation (Buzsáki, 2002).

Conversely, PV interneuron tonic silencing disrupted theta rhythm, decreased the number of PC units per theta cycle, and scattered PC firing during theta cycles. Thus, results from our phasic activation and silencing experiments are in agreement with our tonic activation and silencing experiments and demonstrate that PV interneurons are a crucial component of intrinsic theta oscillators, essential for the proper firing pattern of hippocampal PCs and the emergence of theta oscillations. Altogether, our results provide the first direct demonstration of the capacity of PV interneurons in generating hippocampal theta oscillations.

SOM Interneurons Modulate TA Inputs

SOM interneurons have long been foreseen as instrumental in hippocampal theta generation (Gloveli et al., 2005) (but see Kispersky et al., 2012). In addition, recent work has demonstrated that SOM interneurons influence the probability of PC burst firing (Lovett-Barron et al., 2012; Royer et al., 2012). In this study, optogenetic activation of SOM interneurons was able to phase-lock intrinsically generated dCA1/SUB oscillation, although this effect was restricted to stimulation frequencies close to the frequency of baseline oscillation. Tonic silencing of SOM interneurons also showed a small but significant effect of SOM interneuron network on theta frequency and power. None of the SOM interneuron optogenetic manipulation performed in this study altered PC firing relative to the field oscillation. Taken together, our findings suggest that SOM interneurons provide only a modest contribution to the generation of intrinsic hippocampal theta.

In contrast, double optogenetic experiments allowing the simultaneous manipulation of TA pathway and SOM interneurons revealed a strong role of SOM interneurons in modulating external inputs. TA pathway activation was able to robustly entrain intrinsic theta oscillators at frequencies of activation similar to or slightly above baseline oscillation frequency. Simultaneous SOM interneuron silencing attenuated the effect of TA fiber activation on the field oscillation, decreased the number of PC units per theta cycle, and delayed the firing of PCs. These results suggest that SOM interneurons could be implicated in a disinhibitory mechanism regulating PC firing. To the best of our knowledge, the morphology, electrophysiological properties, and innervation patterns of SOM-expressing neurons in the SUB are unknown. Our patch-clamp results showed that, unlike dCA1 PCs, SUB PCs are entrained by TA pathway activation. Together with the dampening effect of SOM interneuron silencing on TA pathway-entrained dCA1/SUB oscillations, our results suggest that TA inputs are differentially regulated between SUB and dCA1. A recent study has shown that SOM-positive OLM interneurons in CA1 control the strength of Schaffer

collateral inputs through PC disinhibition (Leão et al., 2012). Our results suggest the existence of a similar mechanism controlling EC inputs in the SUB region.

Recent work has highlighted the ability of the hippocampal network to self-generate theta rhythm (Goutagny et al., 2009; Gu et al., 2013) and suggested that its intrinsic architecture is a series of weakly coupled oscillators (Lubenov and Siapas, 2009; Patel et al., 2012; Colgin, 2013). Identification of the cellular subtypes forming theta oscillators is key in understanding theta rhythm in the brain. The combination of an intact hippocampus preparation spontaneously oscillating at theta frequencies with interneuron optogenetic manipulation has allowed us to unravel the cell types constituting intrinsic theta oscillators. SOM interneurons interact with the TA pathway, modulate intrinsic theta oscillators, but are not necessary to theta rhythm generation in the hippocampus. In contrast, the powerful control of PV interneuron network on hippocampal oscillations supports earlier suggestions that perisomatic inhibition onto dCA1/SUB PCs is a central component to theta rhythm generation (Soltesz and Deschênes, 1993; Cobb et al., 1995; Kamondi et al., 1998). The feedback loop formed by PCs and PV interneurons constitutes the minimal network required for the emergence of hippocampal theta. PV interneurons in vivo are targeted by various internal (CA1 and CA3 collaterals and other local CA1 interneurons) and external (GABAergic neurons from the medial septum) afferents (Wulff et al., 2009). Collectively, our data strongly suggest that PV interneuron network is therefore a powerful local hub controlling theta rhythm in the hippocampus.

EXPERIMENTAL PROCEDURES

Animals and Surgical Procedures

All procedures were approved by the McGill University Animal Care Committee and the Canadian Council on Animal Care. PV-Tom and SOM-Tom pups (obtained from breeding PV-Cre or SOM-Cre mice with Ai9 lox-stop-lox-tdTomato reporter strain) at post-natal day 15 were anesthetized using isoflurane and placed in a stereotaxic frame. An injection needle was lowered just above the hippocampus, and 0.5 to 0.8 μl of AAV-ChETA-eYFP, AAV-ArchT-GFP, or AAV-eYFP Cre-dependent viral vectors was infused at a rate of 0.06 μl/min (injection coordinates: anteroposterior −2.70 mm from bregma, lateral ±3.00 mm, dorsoventral −2.05 mm). Injection coordinates were set to obtain virus expression in both dCA1 and SUB, midway between septal and temporal poles of the preparation. ChETA and ArchT expression were quantified in three mice per strain in a 1 mm total area around the injection site (see Supplemental Experimental Procedures for a detailed protocol of the anatomical quantification). For EC injections, the same volume and infusion rate were used to inject an AAV-CamKIIα-ChETA-eYFP vector (coordinates: anteroposterior −3.00 mm from bregma, lateral ±4.50 mm, dorsoventral −3.95 mm). Pups were returned to their home cage and allowed to recover 2 to 3 weeks after surgery.

Electrophysiological Recordings

Patch-clamp experiments were performed on hippocampus slices (400 μm) 12 to 23 days after viral injection. Direct responses to light of ChETA- or ArchT-positive PV or SOM interneurons or post-synaptic responses in PCs were measured in current-clamp and/or voltage-clamp modes in dCA1 and SUB (see Figures S1, S2, and S5). Intact hippocampus preparations were dissected as previously described (Goutagny et al., 2009). The hippocampus preparation from PV or SOM injected mice (13–24 days after injection) was positioned in the recording chamber, and temperature-controlled artificial cerebrospinal fluid (31°C ± 1°C) was perfused at a high flow rate (20–25 ml/min). The absence of light-induced artifacts was verified prior to each experiment. Recordings were performed at the dCA1/SUB border. For both patch-clamp recordings on slices and field recordings in the intact hippocampus preparation, light was provided by a custom-made light-emitting diode (LED) system in which blue (473 nm) or orange (593 nm) LEDs were coupled to a polymer light guide.

Data Acquisition and Analysis

Patch-clamp recordings were performed with an Axon Multiclamp 700B amplifier (Molecular Devices), and field recordings were performed with a differential amplifier (A-M systems) and an Axon Multiclamp 700B amplifier (Molecular Devices). Patch-clamp analysis was performed using a Clampfit 10 software (Molecular Devices). Field and simultaneous field-MUA recordings were analyzed with custom MATLAB scripts (The MathWorks) using the Chronux package (Bokil et al., 2010) and the CircStat toolbox (Berens, 2009). Statistical analysis was performed using Prism 4 (GraphPad Software), Origin (OriginLab), or custom MATLAB scripts. Statistical tests used are described in the text; all data shown are mean ± SEM, with statistical significance set at $p \leq 0.05$.

SUPPLEMENTAL INFORMATION

Supplemental Information includes Supplemental Experimental Procedures and five figures and can be found with this article online at http://dx.doi.org/10.1016/j.neuron.2015.05.027.

ACKNOWLEDGMENTS

We thank J. Jackson and R. Goutagny for their helpful comments on the manuscript and S. Scodras for technical assistance. We thank Edward Boyden (Massachusetts Institute of Technology) and Karl Deisseroth (Stanford University) for providing constructs. This work was supported by the Canadian Institutes of Health Research. B.A. was supported by postdoctoral fellowships from Fondation Fyssen and from Fonds de la Recherche en Santé du Québec. C.Y.L.H. was supported by a Canada Graduate Scholarship from the Natural Sciences and Engineering Research Council of Canada (NSERC). H.N. was supported by an NSERC Alexander Graham Bell Canada Graduate Scholarship and an O'Brien Foundation Alumni Fellowship Award.

Received: December 31, 2013
Revised: March 26, 2015
Accepted: April 21, 2015
Published: June 3, 2015

REFERENCES

Adhikari, A., Topiwala, M.A., and Gordon, J.A. (2010). Synchronized activity between the ventral hippocampus and the medial prefrontal cortex during anxiety. Neuron *65*, 257–269.

Berens, P. (2009). CircStat: a MATLAB toolbox for circular statistics. J. Stat. Softw. *31*, 1–21.

Berndt, A., Schoenenberger, P., Mattis, J., Tye, K.M., Deisseroth, K., Hegemann, P., and Oertner, T.G. (2011). High-efficiency channelrhodopsins for fast neuronal stimulation at low light levels. Proc. Natl. Acad. Sci. U S A *108*, 7595–7600.

Bokil, H., Andrews, P., Kulkarni, J.E., Mehta, S., and Mitra, P.P. (2010). Chronux: a platform for analyzing neural signals. J. Neurosci. Methods *192*, 146–151.

Buzsáki, G. (2002). Theta oscillations in the hippocampus. Neuron *33*, 325–340.

Cardin, J.A., Carlén, M., Meletis, K., Knoblich, U., Zhang, F., Deisseroth, K., Tsai, L.H., and Moore, C.I. (2009). Driving fast-spiking cells induces gamma rhythm and controls sensory responses. Nature *459*, 663–667.

Cobb, S.R., Buhl, E.H., Halasy, K., Paulsen, O., and Somogyi, P. (1995). Synchronization of neuronal activity in hippocampus by individual GABAergic interneurons. Nature *378*, 75–78.

Colgin, L.L. (2013). Mechanisms and functions of theta rhythms. Annu. Rev. Neurosci. *36*, 295–312.

Empson, R.M., and Heinemann, U. (1995). The perforant path projection to hippocampal area CA1 in the rat hippocampal-entorhinal cortex combined slice. J. Physiol. *484*, 707–720.

Freund, T.F., and Antal, M. (1988). GABA-containing neurons in the septum control inhibitory interneurons in the hippocampus. Nature *336*, 170–173.

Gillies, M.J., Traub, R.D., LeBeau, F.E., Davies, C.H., Gloveli, T., Buhl, E.H., and Whittington, M.A. (2002). A model of atropine-resistant theta oscillations in rat hippocampal area CA1. J. Physiol. *543*, 779–793.

Gloveli, T., Dugladze, T., Rotstein, H.G., Traub, R.D., Monyer, H., Heinemann, U., Whittington, M.A., and Kopell, N.J. (2005). Orthogonal arrangement of rhythm-generating microcircuits in the hippocampus. Proc. Natl. Acad. Sci. U S A *102*, 13295–13300.

Goutagny, R., Jackson, J., and Williams, S. (2009). Self-generated theta oscillations in the hippocampus. Nat. Neurosci. *12*, 1491–1493.

Gu, N., Jackson, J., Goutagny, R., Lowe, G., Manseau, F., and Williams, S. (2013). NMDA-dependent phase synchronization between septal and temporal CA3 hippocampal networks. J. Neurosci. *33*, 8276–8287.

Han, X., Chow, B.Y., Zhou, H., Klapoetke, N.C., Chuong, A., Rajimehr, R., Yang, A., Baratta, M.V., Winkle, J., Desimone, R., and Boyden, E.S. (2011). A high-light sensitivity optical neural silencer: development and application to optogenetic control of non-human primate cortex. Front. Syst. Neurosci. *5*, 18.

Jackson, J., Goutagny, R., and Williams, S. (2011). Fast and slow γ rhythms are intrinsically and independently generated in the subiculum. J. Neurosci. *31*, 12104–12117.

Jackson, J., Amilhon, B., Goutagny, R., Bott, J.B., Manseau, F., Kortleven, C., Bressler, S.L., and Williams, S. (2014). Reversal of theta rhythm flow through intact hippocampal circuits. Nat. Neurosci. *17*, 1362–1370.

Kamondi, A., Acsády, L., Wang, X.J., and Buzsáki, G. (1998). Theta oscillations in somata and dendrites of hippocampal pyramidal cells in vivo: activity-dependent phase-precession of action potentials. Hippocampus *8*, 244–261.

Kispersky, T.J., Fernandez, F.R., Economo, M.N., and White, J.A. (2012). Spike resonance properties in hippocampal O-LM cells are dependent on refractory dynamics. J. Neurosci. *32*, 3637–3651.

Klausberger, T., and Somogyi, P. (2008). Neuronal diversity and temporal dynamics: the unity of hippocampal circuit operations. Science *321*, 53–57.

Kocsis, B., Bragin, A., and Buzsáki, G. (1999). Interdependence of multiple theta generators in the hippocampus: a partial coherence analysis. J. Neurosci. *19*, 6200–6212.

Lapray, D., Lasztoczi, B., Lagler, M., Viney, T.J., Katona, L., Valenti, O., Hartwich, K., Borhegyi, Z., Somogyi, P., and Klausberger, T. (2012). Behavior-dependent specialization of identified hippocampal interneurons. Nat. Neurosci. *15*, 1265–1271.

Leão, R.N., Mikulovic, S., Leão, K.E., Munguba, H., Gezelius, H., Enjin, A., Patra, K., Eriksson, A., Loew, L.M., Tort, A.B., and Kullander, K. (2012). OLM interneurons differentially modulate CA3 and entorhinal inputs to hippocampal CA1 neurons. Nat. Neurosci. *15*, 1524–1530.

Lovett-Barron, M., Turi, G.F., Kaifosh, P., Lee, P.H., Bolze, F., Sun, X.H., Nicoud, J.F., Zemelman, B.V., Sternson, S.M., and Losonczy, A. (2012). Regulation of neuronal input transformations by tunable dendritic inhibition. Nat. Neurosci. *15*, 423–430.

Lovett-Barron, M., Kaifosh, P., Kheirbek, M.A., Danielson, N., Zaremba, J.D., Reardon, T.R., Turi, G.F., Hen, R., Zemelman, B.V., and Losonczy, A. (2014). Dendritic inhibition in the hippocampus supports fear learning. Science *343*, 857–863.

Lubenov, E.V., and Siapas, A.G. (2009). Hippocampal theta oscillations are travelling waves. Nature *459*, 534–539.

Maccaferri, G., and McBain, C.J. (1996). The hyperpolarization-activated current (Ih) and its contribution to pacemaker activity in rat CA1 hippocampal stratum oriens-alveus interneurones. J. Physiol. *497*, 119–130.

O'Keefe, J. (1993). Hippocampus, theta, and spatial memory. Curr. Opin. Neurobiol. *3*, 917–924.

Patel, J., Fujisawa, S., Berényi, A., Royer, S., and Buzsáki, G. (2012). Traveling theta waves along the entire septotemporal axis of the hippocampus. Neuron *75*, 410–417.

Pike, F.G., Goddard, R.S., Suckling, J.M., Ganter, P., Kasthuri, N., and Paulsen, O. (2000). Distinct frequency preferences of different types of rat hippocampal neurones in response to oscillatory input currents. J. Physiol. *529*, 205–213.

Royer, S., Zemelman, B.V., Losonczy, A., Kim, J., Chance, F., Magee, J.C., and Buzsáki, G. (2012). Control of timing, rate and bursts of hippocampal place cells by dendritic and somatic inhibition. Nat. Neurosci. *15*, 769–775.

Seidenbecher, T., Laxmi, T.R., Stork, O., and Pape, H.C. (2003). Amygdalar and hippocampal theta rhythm synchronization during fear memory retrieval. Science *301*, 846–850.

Sohal, V.S., Zhang, F., Yizhar, O., and Deisseroth, K. (2009). Parvalbumin neurons and gamma rhythms enhance cortical circuit performance. Nature *459*, 698–702.

Soltesz, I., and Deschênes, M. (1993). Low- and high-frequency membrane potential oscillations during theta activity in CA1 and CA3 pyramidal neurons of the rat hippocampus under ketamine-xylazine anesthesia. J. Neurophysiol. *70*, 97–116.

Stark, E., Eichler, R., Roux, L., Fujisawa, S., Rotstein, H.G., and Buzsáki, G. (2013). Inhibition-induced theta resonance in cortical circuits. Neuron *80*, 1263–1276.

van Strien, N.M., Cappaert, N.L., and Witter, M.P. (2009). The anatomy of memory: an interactive overview of the parahippocampal-hippocampal network. Nat. Rev. Neurosci. *10*, 272–282.

Varga, C., Golshani, P., and Soltesz, I. (2012). Frequency-invariant temporal ordering of interneuronal discharges during hippocampal oscillations in awake mice. Proc. Natl. Acad. Sci. U S A *109*, E2726–E2734.

Wulff, P., Ponomarenko, A.A., Bartos, M., Korotkova, T.M., Fuchs, E.C., Bähner, F., Both, M., Tort, A.B., Kopell, N.J., Wisden, W., and Monyer, H. (2009). Hippocampal theta rhythm and its coupling with gamma oscillations require fast inhibition onto parvalbumin-positive interneurons. Proc. Natl. Acad. Sci. U S A *106*, 3561–3566.

Ylinen, A., Soltész, I., Bragin, A., Penttonen, M., Sik, A., and Buzsáki, G. (1995). Intracellular correlates of hippocampal theta rhythm in identified pyramidal cells, granule cells, and basket cells. Hippocampus *5*, 78–90.